Density, strain rate and strain effects on mechanical property evolution in polymeric foams

Kapil Bharadwaj Bhagavathula[a], Christopher S Meredith[c], Simon Ouellet[d], Dan L Romanyk[a,b], James David Hogan[a]

[a]*Department of Mechanical Engineering, The University of Alberta, Edmonton, AB T6G 2R3, Canada*
[b]*School of Dentistry, The University of Alberta, Edmonton, AB T6G 1C9, Canada*
[c]*Weapons and Materials Research Directorate, US Army Research Lab, Aberdeen Proving Ground, MD 21005, USA*
[d]*Valcartier Research Centre, Defence Research and Development Canada, Quebec, G3J1X5, Canada*

Abstract

This study presents a comprehensive experimental study of the evolution of Poisson's ratio and tangent modulus of polymeric foams during rate dependant uniaxial compression. In this study, polyurethane foams with densities of 195 kg/m^3, 244 kg/m^3, and 405 kg/m^3 obtained from PORON (XRD series) were examined under uniaxial compression loading at strain rates ranging from 0.001 s^{-1} to 5000 s^{-1}. All compression experiments were coupled with a high-speed camera to enable Digital Image Correlation to measure and visualize deformation strains. These measurements enable us to study mechanical property evolution during compression and provide qualitative description of damage and failure in these materials. A non-linear evolution of Poisson's ratio is observed in-situ in these materials. The compressive stress-strain response is predicted through least square fitting using the Avalle model [1], and model coefficients are found to follow a power-law to scale across strain rates. The stress-strain curves, mechanical property evolution, and scaling coefficients are compared with microstructural parameters of interest such as pore size and wall thickness to inform on damage mechanisms

Email address: bhagavat@ualberta.ca (Kapil Bharadwaj Bhagavathula)

in the material.

Keywords: Strain rate, Density, Microstructure, Compression, Polymeric foam

1. Introduction

To better exploit the energy absorbing capabilities of foams and design next-generation materials, it is important to understand the effect of stress states and strain rates on their mechanical response through experimental and modelling approaches. In the literature, numerical models [2–5] and finite element models [4, 6–8] have been developed to predict the mechanical response of cellular polymers. The development of constitutive models [9–13] enable determination of parameters such as elastic moduli [10, 11], collapse stresses [11], and failure strengths and strains[10], which allow the industry to design better foam materials. In some literature, studies have focused on modelling the yield behavior for polymeric foam materials. For example, Ayyagari et al.[9] define the entire yield surface of a material based on two yield strengths parameters derived from uniaxial compression and uniaxial tension. In a separate study, Deshpande et al.[14] define a multi-axial yield surface to predict plastic yield and elastic buckling behaviour of PVC foams. However, in extreme applications where polymeric foams are used (e.g, helmet liners, armor padding), they are subjected to large strains and high strain rates, where these models cannot be used as they do not predict behavior beyond yield.

In micro-mechanical modeling, elementary physics-based constitutive relations are established for the microstructural behavior. One of the most widely used micromechanical models to predict response of polymeric foams is the Gibson and Ashby model [15] where the porous microstructure is defined in terms of struts and faces. In their study, Gibson and Ashby [15] discuss deformation mechanisms for open-cell foams, where the elastic limit of the cell is reached when one or more sets of struts yields plastically, buckles, or fractures. Although the Gibson and Ashby model [15] has been widely modified in many other studies [16–19], three limitations are noted. First, the mechanism-dependant micromechanical model does not consider the effect of strain rate, which has been noted to affect the activated failure mechanisms in polymeric foams [19–23]. Second, the model assumes idealized and repeated microstructures, which are less common in foams used in most engineering applications [2–5, 24–27]. Third, the micromechanical model of Gibson and Ashby [15], as well as other micromechanical [15, 28, 29] and phenomenological models [12, 14, 30–32], assume either no affect of Poisson's ratio (assume $\nu = 0$) or a constant value. In our study, we will address these limitations through experimental observations utilizing the state-of-the-art in-situ visualization and strain rate dependent phenomenological modelling.

In this paper, we explore the compressive response of porous polymers for a range of densities and strain rates. We focus on studying the evolution of mechanical properties during deformation (e.g., tangent modulus and Poisson's ratio). We are motivated to better understand fundamental relationships between densities and strain rates on the stress-strain responses, which informs phenomenological modelling of these behaviors. This work builds on previous phenomenological models in the literature [1, 11, 33], including those that consider strain rate effects [20, 34–36]. Through this work, we provide a better understanding on the combined effects of density, microstructure, and strain rate on the mechanical response of polymeric foams, including notable discoveries on Poisson's ratio evolution and mechanical response. Altogether, phenomenological models and insights developed in this paper can inform the design of new materials [4, 25] and reduce time for desiging these materials when compared with computationally-expensive finite element modelling [1, 4, 26, 37].

2. Experimental Methods

2.1. Material and Characterization

The materials investigated in this work are open-cell polyurethane foams manufactured by PORON that are used in protection applications such as helmet liners, and armor padding. Three different densities of PORON XRD foams are investigated: a low density foam (LD) of 195 kg/m^3, a medium density foam (MD) of 244 kg/m^3, and a high density foam (HD) of 405 kg/m^3. In this study, polymeric foams are examined under uniaxial compression loading at quasistatic, intermediate, and dynamic strain rates. To ensure consistency across different strain rates in compression testing, and for microstructure characterization, a single nominal sample diameter of 8 *mm* was used for all experiments. The sample thickness was restricted by the as-received sheet thickness of 4.2 *mm* for the LD foam, 3.0 *mm* for the MD foam, and 3.0 *mm* for the HD foam, respectively. The sensitivity of mechanical response to specimen geometry, testing methods, and specimen-size effects are widely discussed in literature [10, 38, 39], and we expect some of them to manifest in our materials.

For microstructure characterization, synchrotron radiation based microcomputed X−ray tomography (XCT) was performed on the polymeric foam samples at the Biomedical Imaging and Therapy (BMIT) facility – Canadian Light Source (CLS) [40] 05ID−2−SOE−1 hutch, Saskatoon, Canada. Shown in Figure 1 are XCT scans of pristine microstructures of the three different density foams. Visually comparing the LD foam on the extreme left to the HD foam on the extreme right in Figure 1, distinct differences in microstructural properties (e.g., pore size and wall thickness), and the number of pores are noted. To inform on microstructural metrics, a MATLAB-based program was developed to perform segmentation on the tomograms to calculate pore sizes and wall thicknesses.

From the microstructure analysis, it is found that the average pore size increased from $32 \pm 30\mu m$ to $60 \pm 55\mu m$ as foam density decreased from $404kg/m^3$ to $195kg/m^3$, and the average wall thicknesses were found to $\sim 11 \pm 10\mu m$ across all the different densities studied in this paper. These microstructure metrics are found to be in agreement with those observed in Figure 1. The detailed algorithm and reconstruction methods used to resolve the microstructural features are discussed by Bhagavathula et al.[41]. Some of the physical and mechanical properties provided by the manufacturer, as well as average pore metrics calculated from reconstruction of the tomograms are listed in Table 1.

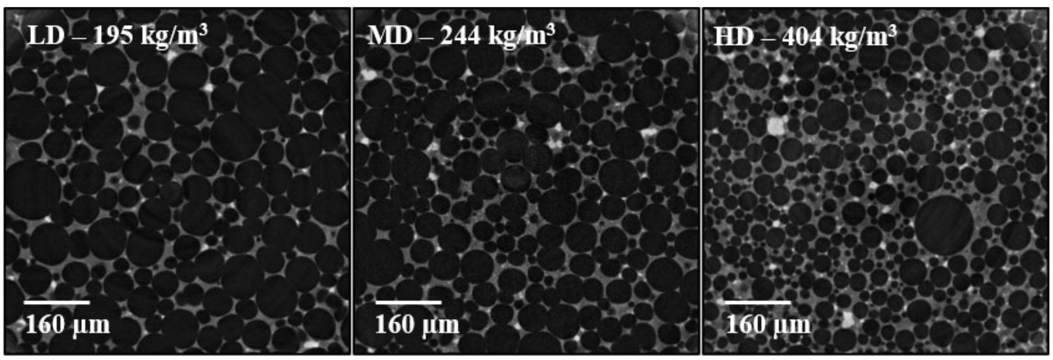

Fig. 1: Pristine microstructures of open-cell polyurethane foams with different densities of 195 kg/m^3 (LD), 244 kg/m^3 (MD), and 405 kg/m^3 (HD) obtained from X-ray tomography scans. The foam material is represented in grey color, and the pore voids are represented by the dark regions.

2.2. Mechanical Testing

2.3. Quasistatic Compression Experiments

The specimens are tested in uniaxial quasistatic compression at strain rates from 0.001 to 0.1 s^{-1} using an E3000 Instron material testing system. A 3 kN load cell with a background noise corresponding to approximately ± 0.01 N recorded the time histories of the forces, and the strains were computed with Digital Image Correlation (discussed later). All quasistatic tests were coupled with a PROMON U750 camera recording at

Table 1: Physical, microstructure and mechanical properties of PORON foams

Property	Test method	Material LD	Material MD	Material HD
Density (specific gravity)	ASTM D 3574-95 Test A[42]	0.19	0.24	0.4
Compressive strength (kPa)	$0.08s^{-1}$@ 25% deflection	8-23	10-38	69-138
Tear Strength min. (kN/m)	ASTM D 624 Die C[43]	0.8	0.8	2.5
Min. Tensile Elongation (%)	ASTM D 3574 Test E[42]	>145	>145	>145
Tensile Strength, min. (kPa)	ASTM D 3574 Test E[42]	207	310	483
Average pore size (μm)	MATLAB Reconstruction[41]	60 ±55	45 ±35	32 ±30
Average wall thickness (μm)	MATLAB Reconstruction[41]	10 ±9	11 ±10	11 ±10
Average porosity (ϕ)	MATLAB Reconstruction[41]	0.87 ±0.06	0.83 ±0.06	0.76 ±0.05

a full resolution of 1280x1024 pixels to visualize deformation features and to perform strain measurements. Both the camera and Instron were set to operate at a sampling rate of 1 frames per second (FPS) for 0.001 s^{-1}, 10 FPS for 0.01 s^{-1}, and 100 FPS for 0.1 s^{-1}. The engineering stresses are calculated by dividing the applied load by the original specimen cross-sectional surface area. Three trials are performed for each density and strain rate to verify repeatability of the material response.

2.4. Intermediate Rate Compression Experiments

Intermediate strain rate compression experiments were performed at two strain rates using different loading techniques. The first strain rate, 1s^{-1}, was performed on an 8871 Instron load frame operating a 1 kN load cell with a background noise corresponding to approximately ±0.01 N. The Instron setup was coupled with a FLIR Grasshopper 3 camera which recorded at 164 FPS. The sample surface was illuminated with a Halogen fiber optic illuminator that ensured good brightness even at high strains. The second intermediate rate was approximately 175 to 250 s^{-1} and utilized a drop tower to reach the necessary strain rates. A PCB 200B04 force sensor with a capacity of 4.45 kN and an upper frequency limit of 75 kHz was attached to a steel base plate, and the sensor had a flat metal loading cap screwed into it that transmitted the force to the quartz sensing element inside the sensor. The foam sample is placed on the loading cap and a metal tup is positioned above the sample at a height of 25 *mm*, and dropped to load the sample. The tup is a relatively heavy metal rod (~4.5 *kg*) compared to the foams, ensuring that the velocity is nominally constant over the loading time. The drop tower setup was coupled with an iX716 high speed camera recording at 20,000 FPS to measure and visualize deformation. The samples were illuminated with multiple halogen fiber optic illuminators to ensure optimum brightness and contrast throughout the experiment. For the intermediate compression tests, the engineering stresses were calculated by dividing the applied load by the original sample area. At least three tests with the similar loading conditions were performed to verify the repeatability of the material response.

2.5. Dynamic Compression Experiments

A modified version of a split-Hopkinson pressure bar (SHPB) apparatus as shown in Figure 2 was used to characterize the dynamic compressive response. The SHPB apparatus had a common diameter of 25.4 *mm* and was made of 6061 aluminum with lengths of 1.2 *m* and 1 *m* for the incident and transmission bars, respectively. 160 GSM paper pulse shapers were used to achieve stress/force equilibrium in the specimens. The use of a paper pulse shaper did not change the rise time or shape of input pulse, but helped minimize high frequency noise in the input wave, and helped achieve acceptable force equilibrium [44]. Two strain-gauges are mounted on diametrically opposite sides of the incident and transmission bars via a bridge configuration to record the strain histories during dynamic compression. The strain gages used in the current setup are $350\Omega \pm 0.3\%$ with a gage factor of $2.130 \pm 0.5\%$ (Micro Measurements CEA-13-250UN-350). The transmitted strain histories are amplified and fed to a GEN3i high-speed data recorder with 16-bit resolution recording at $25MHz$ for data capture and visualization, and trigger control. Under stress equilibrium, the transmitted strain history from the transmission bar, $\epsilon_t(t)$, was used to calculate the engineering stress history $\sigma(t)$ in the samples:

$$\sigma(t) = \frac{A_0}{A_s} E_0 \epsilon_t(t) \textbf{??} \tag{1}$$

where $A_0(m^2)$ and $A_s(m^2)$ are the cross-sectional areas of the bar and sample, respectively, and $E_0(N/m^2)$ is the elastic modulus of the bar material.

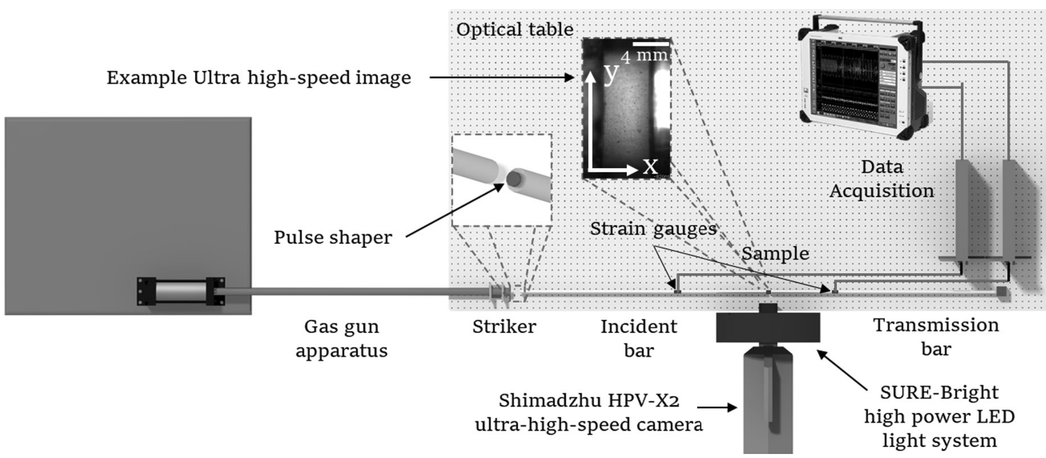

Fig. 2: Modified version of split-Hopkinson Pressure bar apparatus. The arrangement of the ultra-high-speed camera with lens, high power LED light system, and load frame is shown.

In the present study, the dynamic compression experiments were coupled with an ultra-high-speed camera Shimadzu HPV-X2 to visualize deformation features, as well as to perform strain measurements. The camera is able to capture 256 images and is triggered by a split signal from the incident strain-gauge. In these experiments, the camera operated at a frame-rate of 1 million FPS at a resolution of 400x250 pixels. To capture images at such high frame-rates, a SURE-Bright high power LED light system was used to focus an array of light through specialty total internal reflection lenses onto a fixed focal point looking at the specimen. The high intensity continuous light source ensures consistent image quality during acquisition. The camera was triggered from the incident strain-gauge and camera output pulses were used to correlate times between the images and the strain-gauge measurements. The challenges of developing SHPB systems to accurately measure the dynamic response of cellular polymers are well documented in the literature [19, 45–48], and the testing methods that are pursued in the present study are consistent with recommendations from those in previous studies [19, 36, 44].

2.6. Digital Image Correlation (DIC)

In this study, digital image correlation (DIC) was used to measure the strain during experiments. To prepare specimens for DIC analysis, the cylindrical face (orthogonal to the testing axis) is speckle-painted for each specimen. To speckle the specimens, black acrylic ink (Vallejo) is airbrushed (Harder and Steenbeck Infinity airbrush) on the surface to form a speckle pattern for accurate correlation purposes. The VIC-2D 6 software [49] is used for performing DIC analysis on the captured camera images. In DIC analysis, a region of interest (ROI) is manually defined on the speckled surface, and displacements of all the subsets defined within the ROI are tracked as the specimen deforms during loading. Incremental correlation is used for the large deformations experienced during compression. In each time-step, the subsets in the deformed images are "matched" with the pattern in the previous image using the differences in grey scale intensity levels, at each interpolation point. In each subset, a correlation peak is defined by the interpolation of greyscale levels at or between pixels, and the position of the peak provides a local displacement [50]. The test setup was adjusted for every specimen such that images with good sharpness and exposure were obtained providing an optimal subset size in the VIC-2D 6 software.

3. Experimental Results and Discussion

In this section, we will explore the rate-dependent stress-strain response of the three densities of PORON foams. We present stress-strain curve-fits based on constitutive equations derived in the literature for polymeric foams [1], and then detail how these coefficients change as a function of strain rate and density. Then, we give particular attention to tracking the evolution of the mechanical properties during deformation (e.g., tangent modulus and Poisson's ratio).

3.1. Uniaxial Compressive Response

Shown in Figure 3 is a semi-log plot of the strain rate dependent stress-strain curves for each of the three density foams that were tested. Three trials are performed for each condition, but only one representative curve is shown for clarity (we only show a representative curve, but we do use data in Figures 5, 6, 7, and 8). The maximum strain that is measured during these compression experiments is related to when correlation is lost in the DIC computation. Generally, the curves follow similar elastic, plateau, and densification behaviors as has been noted by others [15, 19, 28, 51]. The elastic modulus and collapse stress increase with increasing strain rate and foam density, and this is consistent with the literature [19, 26, 36, 47]. Tabulated measurements of the elastic modulus and collapse stress are found in a previous paper by the authors [52] that explores scaling predictions of these values as a function of strain rate and foam density. In this paper, we give more attention to fitting stress-strain curves to existing models (next section) and to explore the evolution of their elastic properties, especially Poisson's ratio where there have been limited studies. The comprehensive range of strain rates and densities used in this paper augments previous studies in the literature [19, 20, 23, 36, 38, 47, 51, 53, 54].

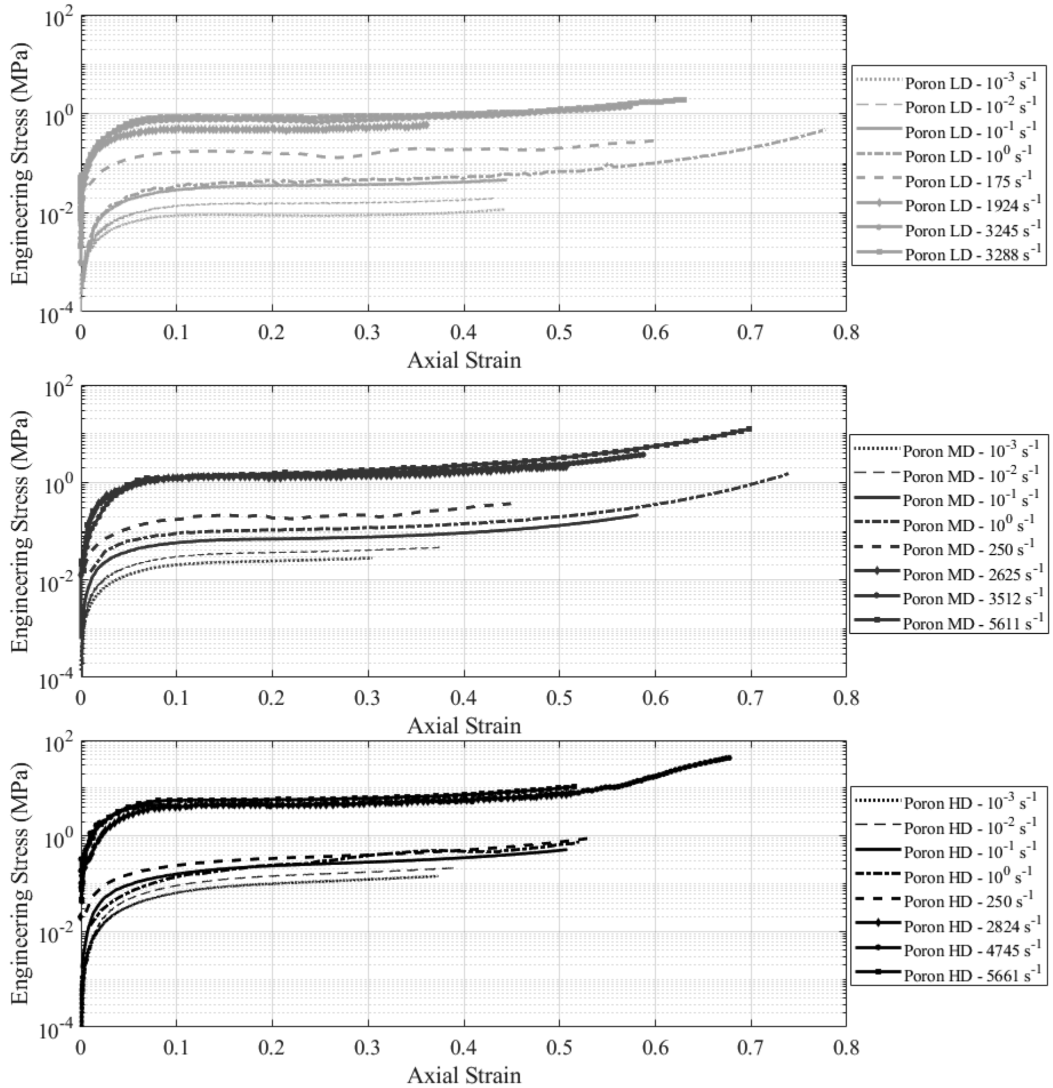

Fig. 3: Experimental results (one representative curve each) for compression tests showing rate effects in PORON foams - (Top) PORON LD foam, (Middle) PORON MD foam, and (Bottom) PORON HD foam. In each sub-figure, the *y*-axis represents stress in megapascals on a logarithmic scale and the *x*-axis represents engineering strain.

3.2. Parameterization of Constitutive Equation

In this sub-section, we apply least-square fit curve fits from existing phenomenological models [1, 20, 33, 35, 36] to better understand how parameters evolve as a function of strain rate and density, and to discuss the applicability of these models to our data. These models are generally expressed as scalar multiples of a shape function and a modulus function [20, 34–36]. The shape function, which is usually a function of strain only, represents the stress-strain relationship at a reference strain rate. The modulus function is a function of both strain and strain rate. The modulus function works as a scale factor for the stress-strain curve between the reference strain rate and another strain rate. First, we present the phenomenological model of Liu and Subhash [33] that was suggested to predict the stress-strain response of polymeric foams. The model has six parameters and is given by:

$$\sigma(\epsilon) = S\,\frac{e^{s\epsilon} - 1}{Q + e^{q\epsilon}} + e^{R}(e^{r\epsilon} - 1) \tag{2}$$

where S, Q, R, s, q and r are empirically fit coefficients from the experimental data. The second model that is explored accounts for strain rate dependency [20, 35, 36], where various models using logarithmic relationships were proposed:

$$P(\dot{\epsilon}) = P(\dot{\epsilon}_0)(1 + k log_{10}(\epsilon/\dot{\epsilon}_0)) \tag{3}$$

where $P(\dot{\epsilon})$ describes the effect of strain rate on various parameters like elastic modulus, collapse stress and energy absorption, k is a constant, and $\dot{\epsilon}_0$ is the reference strain rate. Such relationships have been used to describe both open-cell, and closed-cell foams [20, 35, 36] in the literature. It was found that models described in equations 2 and 3, and similar variations [20, 33, 35, 36] did not fit our data well in terms of under-predicting yield region at high strain rates, and over-predicting densification at lower strain rates. In another study, Avalle et al. [1] proposed a five parameter model which was found to fit our data in all regimes for all strain rates studied in this paper:

$$\sigma(\epsilon) = A(1 - e^{(E/A)\epsilon(1-\epsilon)^m}) + B\left(\frac{\epsilon}{1-\epsilon}\right)^n \tag{4}$$

where the parameters A, E, B, m, and n are empirical parameters. An example of a typical curve fit applied to a medium density foam at a strain rate of 100 s^{-1} and a high density foam at a strain rate of 2255 s^{-1} is shown in Figure 4; we note that the model fits the data well for these and all other density and rate combinations studied in this paper. Here, parameter A controls the magnitude of the plateau stress and can only have a positive value. Parameter E controls the slope of the elastic region and can only be a positive value. Parameter m controls the curvature at yield and can be both positive and negative. Parameter B controls the magnitude of the densification stress and can only be a positive value. Parameter n controls the slope of the densification region and can only be a positive value. Figure 5 shows the variation of these empirical parameters as a function of strain rate for a given density foam material. It is found that parameters A, E, B, and n are density dependent and appear to scale across strain rate using a power-law relationship as follows:

$$P(\dot{\epsilon}) = C\dot{\epsilon}^{\alpha} \tag{5}$$

where $P(\dot{\epsilon})$ is the measured parameter (A, E, B, and n), C is the scaling coefficient, $\dot{\epsilon}$ is the strain rate and α is the power-law exponent. The coefficient m is found to scale via a logarithmic relationship:

$$m = M_1 log(\dot{\epsilon}) + M_2 \tag{6}$$

where M_1 and M_2 are empirical parameters. The coefficients for all the three different densities are tabulated in Table 2, and are determined using a least squares fit. From Table 2, we observe for A and B that the power-law exponent decreases for increasing density, which tells us that lower density materials are prone to higher strain rate effects for the plateau and densification stress magnitudes [55]. For coefficient E, it is observed that the power-law exponent remains consistent throughout the densities suggesting that a single mechanism dominates the elastic response in these materials. This result is in a good agreement with experimental data [56, 57]. Finally, for coefficient n, it is observed that the power-law exponent increases for increasing densities, suggesting that rate of densification is dependant on material density [35, 53].

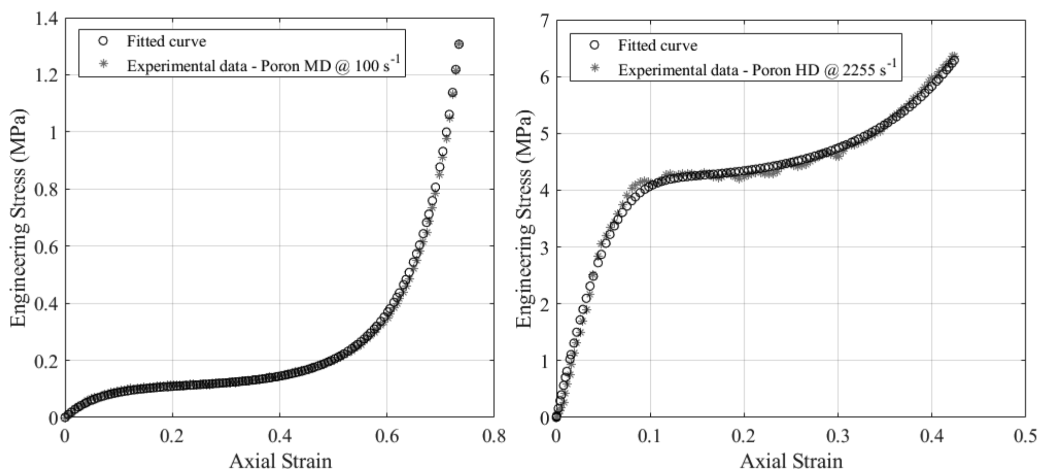

Fig. 4: An example of a typical curve fit: (Left) Medium density PORON at a strain rate of 100 s^{-1}, (Right) High density PORON at a strain rate of 2255 s^{-1}.

3.3. Evolution of Tangent Modulus

Next, we investigate the evolution of the tangent modulus as a function of strain for the different strain rates and densities studied here (Figure 6). We investigate the evolution of the tangent modulus to probe and compare transitional behaviors across the different densities and strain rates. Through these comparisons, we better understand

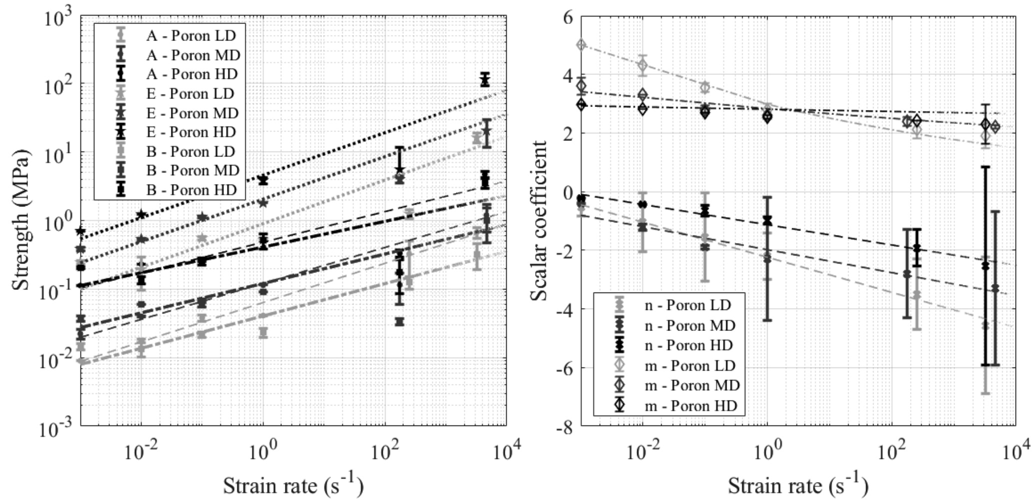

Fig. 5: Trends of model coefficients across varying strain rate for PORON foams (Left) Variation of coefficients *A*, *E* and *B*, (Right) Variation of coefficients *n* and *m*

Table 2: Model coefficients for three density PORON foams for scaling across strain rates

	PORON LD		PORON MD		PORON HD	
	C	α	C	α	C	α
A	0.06	0.28	0.12	0.26	0.48	0.22
E	0.89	0.31	2.05	0.3	4.58	0.31
B	0.04	0.23	0.12	0.21	0.41	0.18
n	2.98	-0.074	2.83	-0.027	2.81	-0.006
	M_1	M_2	M_1	M_2	M_1	M_2
m	-0.26	-2.24	-0.17	-1.98	-0.15	-1.13

damage accumulation mechanisms in the structure and base material during these experiments. In Figure 6, the tangent modulus is computed by using a moving average window filter applied to the stress-strain curves. For the quasi-static experiments, the tangent modulus was averaged over windows of 0.005 to 0.08 strain in size, depending on the number of points and resulting smoothness. For the intermediate strain rate experiments, the tangent modulus was averaged over windows of 0.005 to 0.06 strain. For dynamic strain rates, the tangent modulus was averaged over windows of 0.005 to 0.04 strain. As the strain rate was increased, there were fewer data points to average over, and our choice for the window was influenced by the number of points, range of elastic strain for different strain rates, smoothness of resultant curve, and desire to capture the proper trends and magnitudes. Note that the initial tangent modulus computed through strain-averaged windowing is not necessarily the same value of E that was determined in Figure 5.

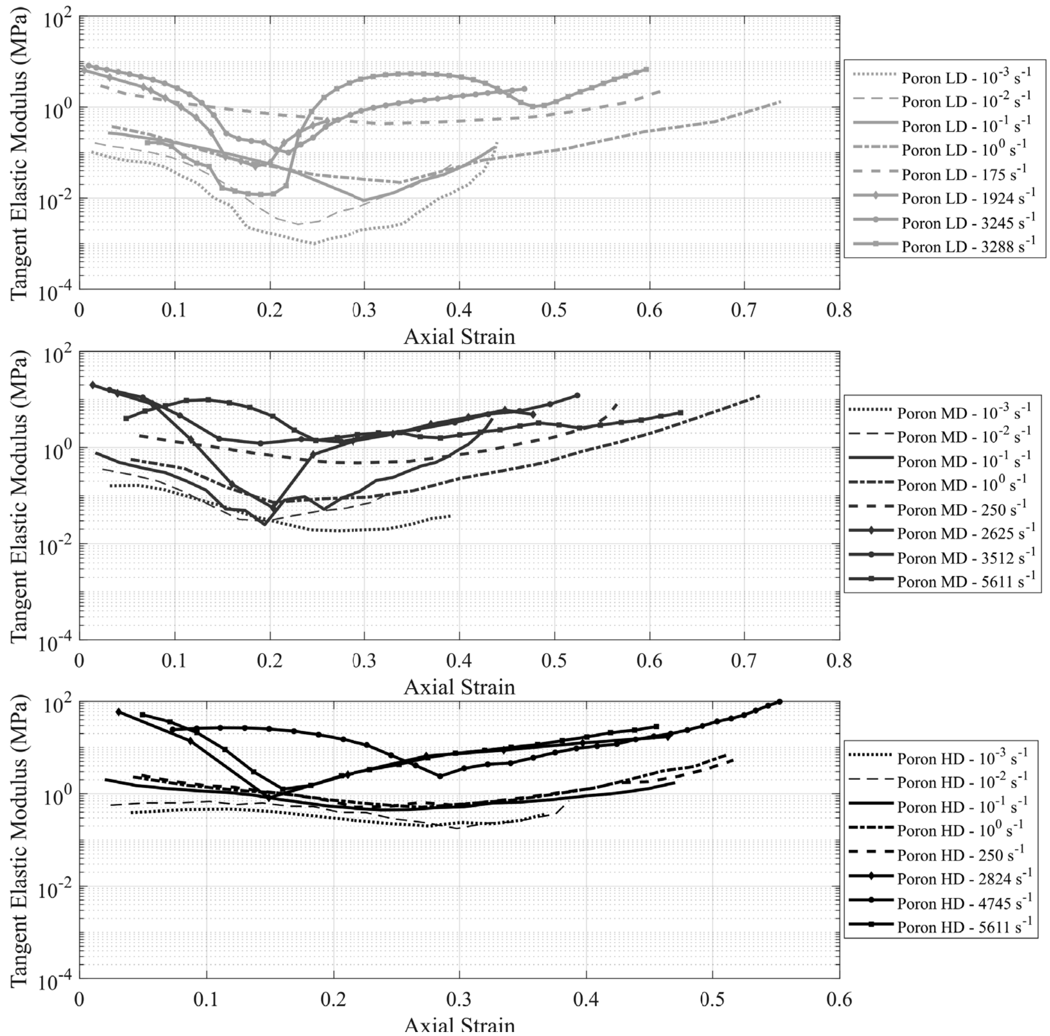

Fig. 6: Evolution of tangent modulus as a function of strain for varying strain rates - (Top) PORON LD foam, (Middle) PORON MD foam, and (Bottom) PORON HD foam.

From Figure 6, we observe that the initial tangent modulus in the elastic regime increase as a function of strain rate and density. In general, the tangent modulus magnitude decreases for increasing strain, with greater sensitivities for higher rates and densities. For all tests, the tangent modulus decreases from its initial value 0 until between 0.2 to 0.3 strain for all the densities with some minor deviations at strain rates > $4500s^{-1}$, after which it begins to increase. These minor deviations are likely a result of manifestation of a transition behavior at higher strain rates. The decrease is likely associated with pore collapse [20, 58, 59], while the increase is likely associated with the onset of cell locking [55, 59]. The relationships between the rate of densification and the density and strain rate were explored previously in evaluating n in Figure 5. The transition behavior of tangent modulus becomes more pronounced at higher dynamic strain rates, and this effect is observed to be common through all the densities studied here. This suggests that the phenomenon is structural in nature, and as strain rate increases, the material has less time to undergo structural deformation as onset of cell locking occurs. This phenomenon is observed to be strain rate dependent as the time available for deformation decreases with increasing strain rate. The lowest point on the curve shifts to the left for increasing strain rate, suggesting the onset of cell locking occurs earlier under higher strain rates [55, 59], with no obvious density effects noted for the materials studied here. This rate-dependent behavior of transitions happening at lower strains (to the right) is likely related to the cell edges having less time to "rearrange" and avoid locking [19, 60], and these trends are consistent with those predicted by previous studies in the literature [59, 61]. Overall from the tangent modulus curves, it is observed that there is no strain range over which the modulus is constant. It is therefore recommended that the tangent modulus should be determined by averaging the measurements from post-zero strain to strains larger than the pore collapse initiation strain, and use this value to represent the elastic modulus of a cellular foam material.

3.4. Evolution of Poisson's Ratio

Finally, we explore the evolution of the Poisson's ratio as a function of strain for the different densities and strain rates (Figure 7). Previous studies have assumed a value of zero [14, 15, 28, 29] or have assumed a constant value for Poisson's ratio in their models [12, 30–32] , whereas utilization of DIC in this paper enables in-situ evolutions to be tracked. In this study, Poisson's ratio is obtained by taking the ratio of the instantaneous lateral strain to the axial strain obtained from the DIC measurements. In Figure 7, we show that Poisson's ratio evolves in a non-monotonic and non-linear manner. For the different density foams, it was found that there is a gradual transition from the elastic to the plateau regime beginning at a strain of $\sim$ 0.02 and plateauing at approximately 0.08 strain, and the limit for the elastic regime was determined as the end of the linear-elastic region in the stress-strain curves. For Poisson's ratio, the values generally *increase* in the elastic regime until yield. For increasing density, there is no obvious trend in how fast the Poisson's ratio increases. The density- and rate-dependent trends in Poisson's ratio are summarized for the elastic regime in Figure 8, which shows that the Poisson's ratio in the elastic regime decreases as a function of strain rate for this current study, with no correlations observed as a function of density. Discussion is, thus, turned back to Figure 7.

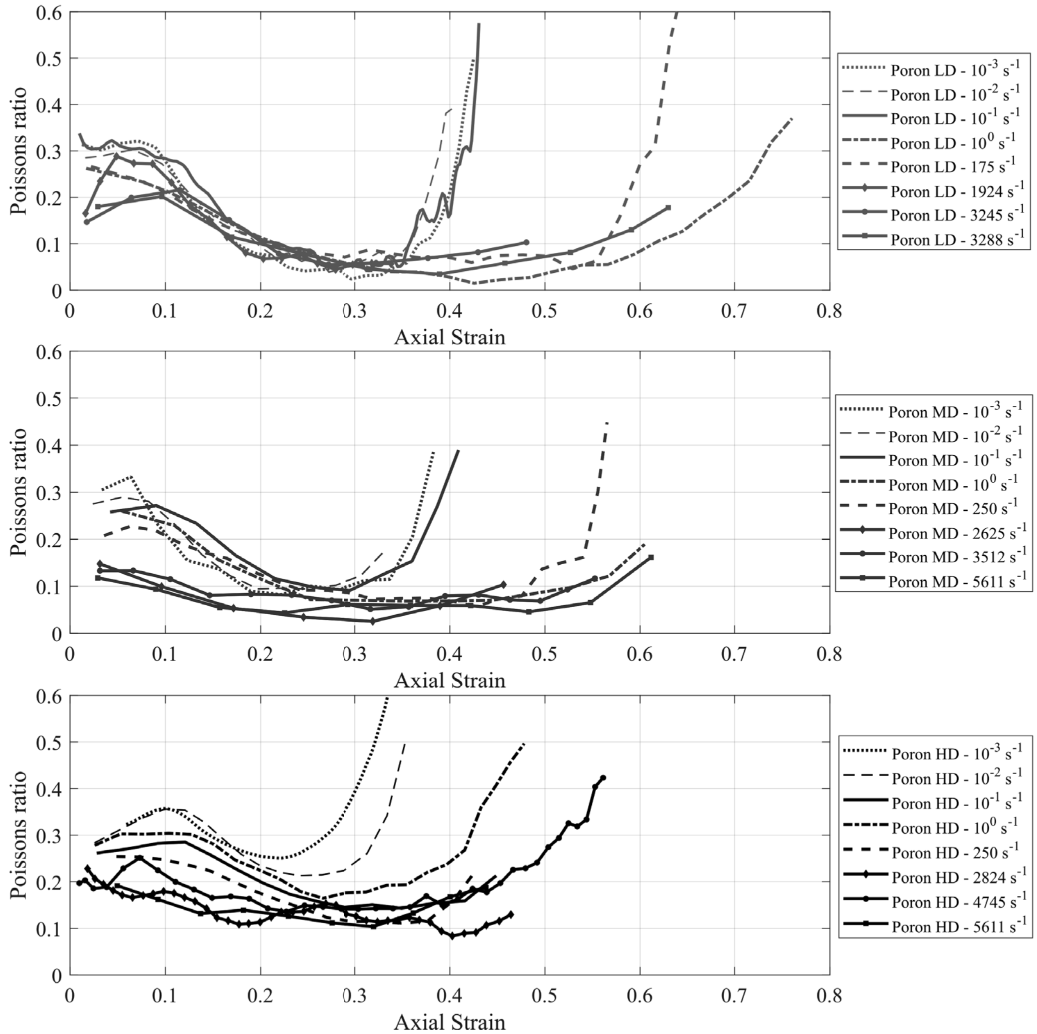

Fig. 7: Evolution of Poisson's ratio as a function of strain for varying strain rates - (Top) PORON LD foam, (Middle) PORON MD foam, and (Bottom) PORON HD foam.

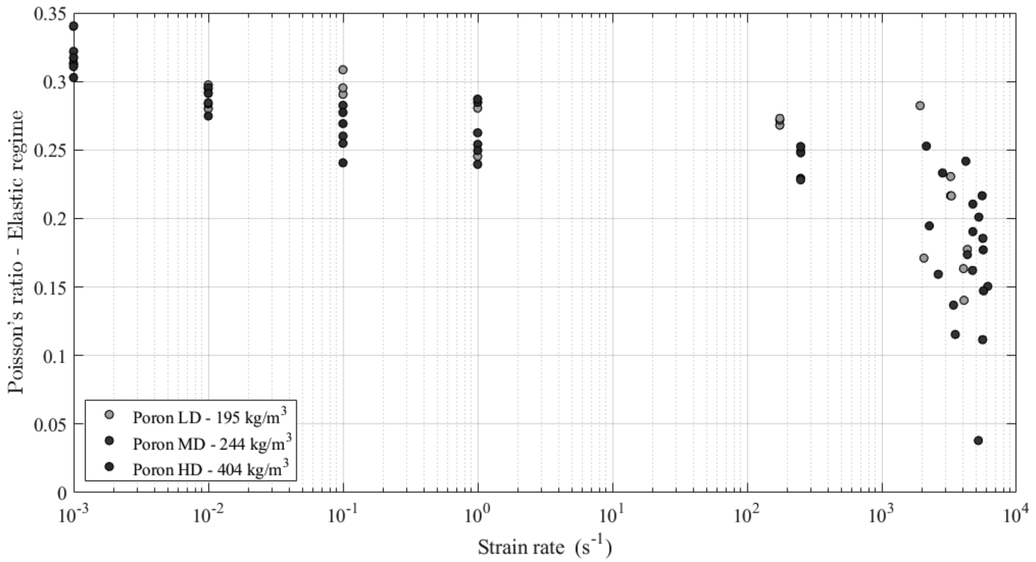

Fig. 8: Variation of the measured Poisson's ratio in the elastic regime under uniaxial compressive loading across varying strain rates for PORON foams of noted densities.

In the elastic regime, it is observed from Figure 7 that Poisson's ratio increases until yield for all materials. The yield limit is observed to shift towards right as density increases up to strains of 0.1 to 0.15. Post-yield and until strains between 0.2 and 0.3, the Poisson's ratio decrease for increasing strain. This is likely related to pore collapse in the material. There is no correlation between density and the value of Poisson's ratio at the lowest points in the Poisson's ratio-strain curves. For increasing strain rate, the rate of decreases in the Poisson's ratio appears to be faster. After decreasing until strains of 0.2 to 0.3, the Poisson's ratio then begins to increase, indicating the onset of pore locking [2, 26]. The strain value at which pore locking occurs shifts to the right for increasing strain rate, indicating that densification may happen later for increasing strain rate. This trend is converse to what was observed in the evolution of the tangent modulus as a function of strain (Figure 6). This highlights the strain rate dependent competition between continued pore collapse that serves to softens the material (captured by Poisson's ratio in Figure 7) and stiffening brought on by cell locking (captured by the tangent modulus in Figure 6). Finally during densification, the rate of increase and magnitude in the Poisson's ratio is greater for higher density foams.

Overall from curves in Figures 6 and 7, it is observed that the minima of tangent modulus happens before minima in Poisson's ratio curves as the stress (manifested in tangent modulus curves) is a precursor to structural deformation (manifested in Poisson's ratio curves). Stated more directly, the stress change always happens before the structure deforms [26]. Minima in tangent modulus curves happens at earlier strains and higher values for increasing strain rate, which corresponds to the structure becoming stiffer for higher rates [20, 47]. Minima in the Poisson's ratio curves happens at higher strains, meaning there is a delay in the onset of structural deformation as rate increases. At high strain rates, tangent modulus and Poisson's ratio evolution is observed to be complex as a consequence of sensitivity of mechanical response to specimen geometry, testing methods, and specimen-size effects as widely discussed in literature [32, 39, 62]. In one study, Sun et al. [59] discuss that the elastic modulus is expected to reduce prior to cell collapse as the cell walls bend and buckle, and this phenomenon is observed in-situ in the present study. This strain rate-dependent response is likely related to an inter-play between structural stiffening, pore sizes that are interrogated, and mechanical properties. This inter-play also manifests as differences in increasing/decreasing trends observed in Figures 6 and 7 as a function of strain, strain rate, and density [10, 38, 39]. This highlights the physical implications for the role of microstructure and density on the evolution of mechanical properties for polymeric foams. These concepts can be extended in the future to other foams to better generalize the approach and determine the model coefficients. The results of the current study can aid others in design and simulation of foam material by considering the following: Commonly, previous foam studies have assumed a value of zero [14, 15, 28, 29] or have assumed a constant value for Poisson's ratio in their models and similar assumptions are observed in many computational models. For more accurate simulations, these higher order models could modify Poisson's ratio as a function of strain rate and microstructure, informed by the data presented here. For foam material design, this observed phenomenon of significant differences in Poisson's ratio between the elastic and plastic phases could be used as an advantage in terms of structural design. This property can inform on deciding the overall shapes and locations of the helmet liners inside a helmet, and where the design commonly balances between comfort (structural deformation) and protection (energy absorption). In the future, the data presented in this paper can be modeled via first principle approaches [8, 58, 63] to fully develop a strain rate-dependant constitutive model, but we do not do it here because it is more impactful when multiple stress-state experiments are performed.

4. Conclusion

In this study, polyurethane foams of three different densities (195 kg/m^3, 244 kg/m^3, 405 kg/m^3) obtained from PORON were examined under uniaxial compression loading at varying strain rates from 0.001 s^1 to 5000 s^1. All compression experiments were coupled with a high-speed camera to measure and visualize deformation. Digital image correlation was performed to obtain deformation and mechanical property evolution characteristics (e.g., tangent modulus and Poisson's ratio). The rate dependent compressive response was fit to the Avalle model [1] and model coefficients were found to follow a power-law. Evolution of damage is studied in terms of in-situ measurements of tangent modulus and Poisson's ratio. Overall, this study addresses some of the limitations that are noted in literature such as lack of consideration for the effect of strain rate, and the effect of Poisson's ratio during loading. In this study, we address this gap by investigating mechanical properties and failure behavior for a wide range of strain rates alongside comparing with microstructure properties. These kind of in-situ measurements are shown for the first time and these measurements are motivated by looking at the evolution of these properties to learn about transitional behaviours. This study also provides a comprehensive set of data to better populate experimental data across varying densities and strain rates, provide data to models, recognize many modeling methods and resources to parameterize the models.

5. Acknowledgments

This research was sponsored by the Army Research Laboratory and was accomplished under Cooperative Agreement Number W911NF-16-2-0083. The views and conclusions contained in this document are those of the authors and should not be interpreted as representing the official policies, either expressed or implied, of the Army Research Laboratory or the U.S. Government. The authors also acknowledge Michael Harr and Paul Moy from US Army Research Laboratory for their help with experimentation. The U.S. Government is authorized to reproduce and distribute reprints for Government purposes notwithstanding any copyright notation herein. Research described in this paper was performed at the BMIT facility at the Canadian Light Source, which is supported by the Canada Foundation for Innovation, Natural Sciences and Engineering Research Council of Canada, the University of Saskatchewan, the Government of Saskatchewan, Western Economic Diversification Canada, the National Research Council Canada, and the Canadian Institutes of Health Research. We also greatly acknowledge the in-kind support of Defence Research and Development Canada. We also thank Mitul Patel of Department of Mechanical Engineering, University of Alberta for his

help with experimental setup.

6. References

References

[1] M. Avalle, G. Belingardi, and A. Ibba, “Mechanical models of cellular solids: Parameters identification from experimental tests,” *International Journal of Impact Engineering*, vol. 34, no. 1, pp. 3–27, jan 2007. [Online]. Available: http://linkinghub.elsevier.com/retrieve/pii/S0734743X06001023

[2] A. D. Brydon, S. G. Bardenhagen, E. A. Miller, and G. T. Seidler, “Simulation of the densification of real open-celled foam microstructures,” *Journal of the Mechanics and Physics of Solids*, vol. 53, no. 12, pp. 2638–2660, 2005.

[3] Z. Nie, Y. Lin, and Q. Tong, “Modeling structures of open cell foams,” *Computational Materials Science*, vol. 131, pp. 160–169, 2017. [Online]. Available: http://dx.doi.org/10.1016/j.commatsci.2017.01.029

[4] W. Y. Jang, A. M. Kraynik, and S. Kyriakides, “On the microstructure of open-cell foams and its effect on elastic properties,” *International Journal of Solids and Structures*, vol. 45, no. 7-8, pp. 1845–1875, 2008.

[5] J. J. Timothy and G. Meschke, “A cascade continuum micromechanics model for the effective elastic properties of porous materials,” *International Journal of Solids and Structures*, vol. 83, pp. 1–12, apr 2016. [Online]. Available: https://linkinghub.elsevier.com/retrieve/pii/S0020768315005028

[6] S. Youssef, E. Maire, and R. Gaertner, “Finite element modelling of the actual structure of cellular materials determined by X-ray tomography,” *Acta Materialia*, vol. 53, no. 3, pp. 719–730, 2005.

[7] R. Huang, P. Li, and T. Liu, “X-ray microtomography and finite element modelling of compressive failure mechanism in cenosphere epoxy syntactic foams,” *Composite Structures*, vol. 140, pp. 157–165, 2016. [Online]. Available: http://dx.doi.org/10.1016/j.compstruct.2015.12.040

[8] J. Zhang, N. Kikuchi, V. Li, A. Yee, and G. Nusholtz, “Constitutive modeling of polymeric foam material subjected to dynamic crash loading,” *International Journal of Impact Engineering*, vol. 21, no. 5, pp. 369–386, 1998. [Online]. Available: http://linkinghub.elsevier.com/retrieve/pii/S0734743X97000870

[9] R. S. Ayyagari and M. Vural, “Multiaxial yield surface of transversely isotropic foams: Part I—Modeling,” *Journal of the Mechanics and Physics of Solids*, vol. 74, no. 2015, pp. 49–67, jan 2015.

[10] M. E. Kabir, M. C. Saha, and S. Jeelani, “Tensile and fracture behavior of polymer foams,” *Materials Science and Engineering A*, vol. 429, no. 1-2, pp. 225–235, 2006.

[11] T. R. Walter, A. W. Richards, and G. Subhash, “A Unified Phenomenological Model for Tensile and Compressive Response of Polymeric Foams,” *Journal of Engineering Materials and Technology*, vol. 131, no. 1, p. 011009, 2009. [Online]. Available: http://materialstechnology.asmedigitalcollection.asme.org/article.aspx?articleid=1428331

[12] M. Shafiq, R. S. Ayyagari, M. Ehaab, and M. Vural, "Multiaxial yield surface of transversely isotropic foams: Part II - Experimental," *Journal of the Mechanics and Physics of Solids*, vol. 76, no. 2015, pp. 224–236, 2015.

[13] C. M. Ford and L. J. Gibson, "Uniaxial strength asymmetry in cellular materials: An analytical model," *International Journal of Mechanical Sciences*, vol. 40, no. 6, pp. 521–531, 1998.

[14] V. S. Deshpande and N. A. Fleck, "Multi-axial yield behaviour of polymer foams," *Acta Materialia*, vol. 49, no. 10, pp. 1859–1866, 2001.

[15] M. F. Ashby, "The properties of foams and lattices," *Philosophical Transactions of the Royal Society A: Mathematical, Physical and Engineering Sciences*, vol. 364, no. 1838, pp. 15–30, 2006.

[16] J. Zhang, Q. Qin, X. Han, and W. Ai, "The initial plastic failure of fully clamped geometrical asymmetric metal foam core sandwich beams," *Composites Part B: Engineering*, vol. 87, pp. 233–244, 2016. [Online]. Available: http://dx.doi.org/10.1016/j.compositesb.2015.10.027

[17] N. J. Mills, R. Stämpfli, F. Marone, and P. A. Brühwiler, "Finite element micromechanics model of impact compression of closed-cell polymer foams," *International Journal of Solids and Structures*, vol. 46, no. 3-4, pp. 677–697, 2009. [Online]. Available: http://dx.doi.org/10.1016/j.ijsolstr.2008.09.012

[18] A. M. Kraynik, M. K. Neilsen, D. A. Reinelt, and W. E. Warren, "Foam micromechanics," pp. 259–286, 1997.

[19] M. C. Saha, H. Mahfuz, U. K. Chakravarty, M. Uddin, M. E. Kabir,

and S. Jeelani, “Effect of density, microstructure, and strain rate on compression behavior of polymeric foams,” *Materials Science and Engineering A*, vol. 406, no. 1-2, pp. 328–336, oct 2005. [Online]. Available: http://linkinghub.elsevier.com/retrieve/pii/S0921509305006830

[20] B. Song, W. W. Chen, S. Dou, N. A. Winfree, and J. H. Kang, “Strain-rate effects on elastic and early cell-collapse responses of a polystyrene foam,” *International Journal of Impact Engineering*, vol. 31, no. 5, pp. 509–521, 2005.

[21] L. Cui, S. Kiernan, and M. D. Gilchrist, “Designing the energy absorption capacity of functionally graded foam materials,” *Materials Science and Engineering A*, vol. 507, no. 1-2, pp. 215–225, 2009.

[22] D. Dattelbaum, D. Robbins, R. Gustavsen, S. Sheffield, D. Stahl, and J. Coe, “Shock compression of polyurethane foams,” *EPJ Web of Conferences*, vol. 26, p. 02014, 2012. [Online]. Available: http://dx.doi.org/10.1051/epjconf/20122602014

[23] G. Subhash, Q. Liu, and X. L. Gao, “Quasistatic and high strain rate uniaxial compressive response of polymeric structural foams,” *International Journal of Impact Engineering*, vol. 32, no. 7, pp. 1113–1126, jul 2006.

[24] S. Gaitanaros and S. Kyriakides, “On the effect of relative density on the crushing and energy absorption of open-cell foams under impact,” *International Journal of Impact Engineering*, vol. 82, pp. 3–13, 2015. [Online]. Available: http://dx.doi.org/10.1016/j.ijimpeng.2015.03.011

[25] M. S. Gholami, O. Doutres, and N. Atalla, “Effect of microstructure closed-pore content on the mechanical properties of flexible polyurethane foam,” *International*

Journal of Solids and Structures, vol. 112, pp. 97–105, 2017. [Online]. Available: http://dx.doi.org/10.1016/j.ijsolstr.2017.02.016

[26] Y. Sun and Q. M. Li, “Dynamic compressive behaviour of cellular materials: A review of phenomenon, mechanism and modelling,” *International Journal of Impact Engineering*, vol. 112, no. October 2017, pp. 74–115, 2018.

[27] N. Mills, “Polyurethane foams: processing and microstructure,” pp. 19–37, 2007. [Online]. Available: https://linkinghub.elsevier.com/retrieve/pii/B9780750680691500039

[28] L. J. Gibson and M. F. Ashby, “The Mechanics of Three-Dimensional Cellular Materials,” *Proceedings of the Royal Society A: Mathematical, Physical and Engineering Sciences*, vol. 382, no. 1782, pp. 43–59, jul 1982. [Online]. Available: http://rspa.royalsocietypublishing.org/cgi/doi/10.1098/rspa.1982.0088

[29] D. V. W. M. de Vries, “Characterization of polymeric foams,” Ph.D. dissertation, Eindhoven University of Technology, 2009.

[30] N. J. Mills and H. X. Zhu, “The high strain compression of closed-cell polymer foams,” *Journal of the Mechanics and Physics of Solids*, vol. 47, no. 3, pp. 669–695, 1999. [Online]. Available: http://linkinghub.elsevier.com/retrieve/pii/S0022509698000076

[31] P. Viot and A. Mercier, “Behaviour of Polymeric Multiscale Foam Under Dynamic Loading -Study of the Influence of the Density and the Walls of Beads,” vol. 7, no. April, pp. 1–19, 2011.

[32] B. Sanborn and B. Song, “Poisson’s ratio of a hyperelastic foam under

quasi-static and dynamic loading," *International Journal of Impact Engineering*, vol. 123, no. May 2018, pp. 48–55, 2019. [Online]. Available: https://doi.org/10.1016/j.ijimpeng.2018.06.001

[33] Q. Liu and G. Subhash, "A phenomenological constitutive model for foams under large deformations," *Polymer Engineering and Science*, vol. 44, no. 3, pp. 463–473, 2004.

[34] J. A. Sherwood and C. C. Frost, "Constitutive modeling and simulation of energy absorbing polyurethane foam under impact loading," *Polymer Engineering & Science*, vol. 32, no. 16, pp. 1138–1146, 1992.

[35] I. M. Daniel, J. M. Cho, and B. T. Werner, "Characterization and modeling of stain-rate-dependent behavior of polymeric foams," *Composites Part A: Applied Science and Manufacturing*, vol. 45, pp. 70–78, 2013. [Online]. Available: http://dx.doi.org/10.1016/j.compositesa.2012.10.003

[36] S. Koumlis and L. Lamberson, "Strain Rate Dependent Compressive Response of Open Cell Polyurethane Foam," *Experimental Mechanics*, may 2019. [Online]. Available: http://link.springer.com/10.1007/s11340-019-00521-3

[37] D. Niedziela, I. E. Ireka, and K. Steiner, "Computational Analysis of Nonuniform Expansion in Polyurethane Foams," *Polymers*, vol. 11, no. 1, p. 100, 2019.

[38] D. S. Cronin and S. Ouellet, "Low density polyethylene, expanded polystyrene and expanded polypropylene: Strain rate and size effects on mechanical properties," *Polymer Testing*, vol. 53, pp. 40–50, aug 2016.

[39] I. Carranza, A. D. Crocombe, I. Mohagheghian, P. A. Smith, A. Sordon,

G. Meeks, and C. Santoni, “Characterising and modelling the mechanical behaviour of polymeric foams under complex loading,” *Journal of Materials Science*, vol. 54, no. 16, pp. 11 328–11 344, 2019. [Online]. Available: https://doi.org/10.1007/s10853-019-03673-8

[40] T. W. Wysokinski, D. Chapman, G. Adams, M. Renier, P. Suortti, and W. Thomlinson, “Beamlines of the biomedical imaging and therapy facility at the Canadian light source - Part 3,” *Nuclear Instruments and Methods in Physics Research, Section A: Accelerators, Spectrometers, Detectors and Associated Equipment*, vol. 775, pp. 1–4, 2015.

[41] K. Bhagavathula, J. Parcon, A. Azar, S. Ouellet, S. Satapathy, C. Dennison, and J. Hogan, “Quasistatic response of a shear-thickening foam: Microstructure evolution and infrared thermography,” *Journal of Cellular Plastics*, 2020.

[42] S. T. Methods, “Standard Test Methods for Flexible Cellular Materials — Slab , Bonded , and Molded Urethane Foams,” *Astm*, vol. Designatio, no. January, pp. 1–29, 2012.

[43] A. D. 624-00, “Standard Test Method for Tear Strength of Conventional Vulcanized Rubber and,” *Annual Book of ASTM Standards*, vol. 00, no. Reapproved, pp. 1–9, 2012.

[44] K. B. Bhagavathula, A. Azar, S. Ouellet, S. Satapathy, C. R. Dennison, and J. D. Hogan, “High Rate Compressive Behaviour of a Dilatant Polymeric Foam,” *Journal of Dynamic Behavior of Materials*, vol. 4, no. 4, pp. 573–585, dec 2018. [Online]. Available: http://dx.doi.org/10.1007/s40870-018-0176-0 http://link.springer.com/10.1007/s40870-018-0176-0

[45] G. T. Gray and W. R. Blumenthal, “Split-Hopkinson Pressure Bar Testing of Soft Materials,” *Mechanical Testing and Evaluation*, vol. 8, pp. 488–496, 2018.

[46] A. Ajdari, H. Nayeb-Hashemi, and A. Vaziri, “Dynamic crushing and energy absorption of regular, irregular and functionally graded cellular structures,” *International Journal of Solids and Structures*, vol. 48, no. 3-4, pp. 506–516, 2011. [Online]. Available: http://dx.doi.org/10.1016/j.ijsolstr.2010.10.018

[47] R. Bouix, P. Viot, and J. L. Lataillade, “Polypropylene foam behaviour under dynamic loadings: Strain rate, density and microstructure effects,” *International Journal of Impact Engineering*, vol. 36, no. 2, pp. 329–342, feb 2009. [Online]. Available: http://linkinghub.elsevier.com/retrieve/pii/S0734743X08000791

[48] J. Lankford and K. A. Dannemann, “Strain Rate Effects in Porous Materials,” *MRS Proceedings*, vol. 521, pp. 103–108, 1998.

[49] Vic-2d, correlated solutions inc, irmo, south carolina, vic-2d. [Online]. Available: https://www.correlatedsolutions.com/vic-2d/

[50] H. S. Michael A. Sutton, Jean Jose Orteu, *Image Correlation for Shape, Motion and Deformation Measurements*. New York, NY: Springer US, 2009. [Online]. Available: https://www.springer.com/gp/book/9780387787466

[51] S. Ouellet, D. Cronin, and M. Worswick, “Compressive response of polymeric foams under quasi-static, medium and high strain rate conditions,” *Polymer Testing*, vol. 25, no. 6, pp. 731–743, sep 2006. [Online]. Available: http://linkinghub.elsevier.com/retrieve/pii/S0142941806000973

[52] K. Bhagavathula, C. Meredith, S. Satapathy, S. Ouellet, D. Romanyk, , and

J. Hogan, “Density, microstructure and strain-rate effects on the compressive response of polyurethane foams,” *Experimental Mechanics*, 2021.

[53] W. Chen, F. Lu, and N. Winfree, “High-strain-rate compressive behavior of a rigid polyurethane foam with various densities,” *Experimental Mechanics*, vol. 42, no. 1, pp. 65–73, 2002.

[54] B. Song, W. Chen, and D. J. Frew, “Dynamic compressive response and failure behavior of an epoxy syntactic foam,” *Journal of Composite Materials*, vol. 38, no. 11, pp. 915–936, jun 2004. [Online]. Available: http://journals.sagepub.com/doi/10.1177/0021998304040552

[55] S. Deschanel, L. Vanel, N. Godin, E. Maire, G. Vigier, and S. Ciliberto, “Mechanical response and fracture dynamics of polymeric foams,” *Journal of Physics D: Applied Physics*, vol. 42, no. 21, 2009.

[56] V. A. Kuzkin, “Structural model for the dynamic buckling of a column under constant rate compression,” pp. 1–8, jun 2015. [Online]. Available: http://arxiv.org/abs/1506.00427

[57] B. Erickson, K. Mimura, T. Kikui, N. Nishide, T. Umeda, I. Riku, and H. Hashimoto, “Buckling behavior of clamped and intermediately-supported long rods in the static–dynamic transition velocity region,” *J. Soc. Mater. Sci.*, vol. 61, no. 11, pp. 881–887, 2012.

[58] J.-H. Lee, D.-M. Ryu, and C.-S. Lee, “Constitutive-damage modeling and computational implementation for simulation of elasto-viscoplastic-damage behavior of polymeric foams over a wide range of strain rates and temperatures,”

International Journal of Plasticity, vol. 130, no. February, p. 102712, jul 2020. [Online]. Available: https://doi.org/10.1016/j.ijplas.2020.102712 https://linkinghub.elsevier.com/retrieve/pii/S0749641919305418

[59] Y. Sun, B. Amirrasouli, S. B. Razavi, Q. M. Li, T. Lowe, and P. J. Withers, “The variation in elastic modulus throughout the compression of foam materials,” *Acta Materialia*, vol. 110, pp. 161–174, 2016.

[60] B. Koohbor, S. Ravindran, and A. Kidane, “Effects of cell-wall instability and local failure on the response of closed-cell polymeric foams subjected to dynamic loading,” *Mechanics of Materials*, vol. 116, pp. 67–76, 2018.

[61] E. Flores-Johnson, Q. Li, and R. Mines, “Degradation of elastic modulus of progressively crushable foams in uniaxial compression,” *Journal of cellular plastics*, vol. 44, no. 5, pp. 415–434, 2008.

[62] B. M. Patterson, N. L. Cordes, K. Henderson, J. J. Williams, T. Stannard, S. S. Singh, A. R. Ovejero, X. Xiao, M. Robinson, and N. Chawla, “In situ X-ray synchrotron tomographic imaging during the compression of hyper-elastic polymeric materials,” *Journal of Materials Science*, vol. 51, no. 1, pp. 171–187, 2015.

[63] E. Ghorbel, “A viscoplastic constitutive model for polymeric materials,” *International Journal of Plasticity*, vol. 24, no. 11, pp. 2032–2058, 2008.